ACS Catalysis

Research Article

Cite This: ACS Catal. 2019, 9, 6243−6251

pubs.acs.org/acscatalysis

Cu−Al Spinel as a Highly Active and Stable Catalyst for the Reverse Water Gas Shift Reaction

Ali M. Bahmanpour,[†] Florent Héroguel,[†] Murat Kılıç,[†] Christophe J. Baranowski,[†] Luca Artiglia,[‡] Ursula Röthlisberger,[†] Jeremy S. Luterbacher,[†] and Oliver Kröcher*[,†,‡]

[†]Institute of Chemical Sciences and Engineering, École Polytechnique Fédérale de Lausanne (EPFL), 1015 Lausanne, Switzerland

[‡]Paul Scherrer Institut (PSI), 5232 Villigen, Switzerland

Supporting Information

ABSTRACT: The reverse water gas shift reaction is considered to be a highly attractive catalytic route for CO_2 recycling in a future sustainable economy. Copper-based catalysts are commonly used for this reaction due to their high activity and selectivity. However, their low thermal stability is problematic for long-term usage. Here, we introduce an in situ formed surface Cu−Al spinel as a highly active and stable catalyst for the reverse water gas shift reaction. Even at high weight hourly space velocities (300 000 mL g^{-1} h^{-1}), we observed no detectable deactivation after 40 h of operation. Through in situ DRIFTS and DFT studies, it was found that 2-fold coordinated copper ions and 3-fold coordinated surface oxygen atoms constitute the active sites for this reaction.

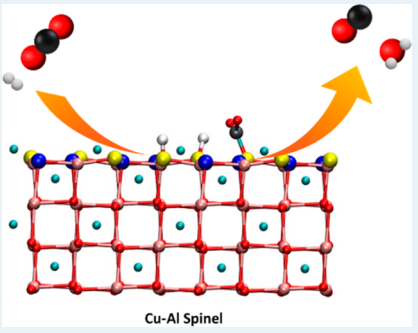

KEYWORDS: *CO_2 hydrogenation, copper, spinel, metal−support interaction, stability*

INTRODUCTION

The effects of excessive CO_2 emissions on climate change have initiated a global search for efficient CO_2 capture and utilization systems.[1,2] Among them, catalytic CO_2 hydrogenation has recently generated high interest as a promising way to convert the constantly increasing emitted CO_2 to fuels and chemicals.[3] Although the process of direct CO_2 conversion to value-added chemicals, such as methanol and formic acid, has shown promising progress,[4] it still remains a challenging step due to the thermodynamic stability of CO_2. Catalytic CO_2 hydrogenation to CO, also known as the reverse water gas shift (RWGS) reaction, is recognized as a promising and important option for CO_2 valorization. Advanced industrial processes for CO conversion to energy-rich chemicals have been used for a long time, and the catalytic conversion of CO is well-studied.[5,6] Moreover, CO formation is known to be an important intermediate step in CO_2 hydrogenation reactions.[7,8] Therefore, further improvement of the RWGS reaction can effectively boost the carbon recycling system. Recently, many studies have focused on catalyst improvement for the RWGS reaction.[9−12] Copper, gold, and platinum are known to be the main active metals for this reaction. Considering high CO selectivity and activity of copper,[11] as well as its low cost compared to gold and platinum, copper-based catalysts may be the most promising candidates for use in the RWGS reaction. However, low thermal stability of copper at high temperatures and, therefore, its rapid deactivation due to sintering and reoxidation are the main drawbacks of this catalyst.[2] Many researchers have attempted to stabilize copper using various promoters and/or supports.[11,13,14] However, all of these studies have encountered a trade-off between CO yield, WHSV, and/or stability, where insufficient performance with respect to at least one of these parameters has prevented the implementation of their catalysts. Through coprecipitation of copper and aluminum followed by hydrogen treatment, we obtained an in situ synthesized surface Cu−Al spinel, which proved to have not only remarkable stability but also a much higher activity compared to any other copper-based heterogeneous catalyst described so far for the RWGS reaction.

RESULTS AND DISCUSSION

Coprecipitation or impregnation followed by high-temperature calcination (>900 °C) have been reported for the formation of spinels.[15,16] Some of these spinel-type catalysts were shown to be active in the methanol steam reforming and water gas shift (WGS) reaction.[17−19] However, high-temperature calcination can reduce the surface area of the synthesized spinel.[16] Bolt et al. stated that surface Cu−Al spinel formation can be initiated at relatively low temperatures (500 °C) and accelerated in the presence of steam.[20] Low-temperature surface spinel formation was reported in the literature through hydrogen treatment.[21] Hydrogen treatment can in fact form steam, which helps the surface Cu−Al spinel formation process without decreasing its surface area. Here, we used coprecipitation followed by hydrogen treatment to form a surface Cu−Al spinel with high surface area. Various nCu−Al_2O_3 catalysts were prepared

Received: May 3, 2019
Revised: May 29, 2019
Published: June 3, 2019

DOI: 10.1021/acscatal.9b01822
ACS Catal. 2019, 9, 6243−6251

by coprecipitation with Cu/Al nominal molar ratios of 1, 2, and 3, which hereafter are noted as 2Cu−Al_2O_3, 4Cu−Al_2O_3, and 6Cu−Al_2O_3, respectively. A Cu/Al_2O_3 catalyst (4 wt % Cu prepared by wet impregnation) served as the reference material. Actual Cu/Al molar ratio, BET surface area (S_{BET}), pore volume (V_p), and crystalline size were measured for all catalysts (Table 1). The Cu−Al catalysts were screened for the RWGS reaction at various temperatures, the results of which are presented in Figure S1 (Supporting Information, relative characterization data in Figures S2−S4). In these tests, 4Cu−Al_2O_3 showed the highest activity even at high WHSV values of 300 000 mL g^{-1} h^{-1} (Figures S1 and S5). It can be seen in the STEM-EDXS images (Figure S6) that the CuO islands formed in 2Cu−Al_2O_3 were relatively large and were not uniformly mixed with the Al_2O_3 phase. Cu entities in 6Cu−Al_2O_3, however, were mostly present in the catalyst bulk rather than the surface (Table S1). Coverage of the surface by the Al_2O_3 phase can also be noted in Figure S6c. Only in 4Cu−Al_2O_3 were a homogeneous distribution of CuO and Al_2O_3 phases observed. It is plausible to assume that this characteristic together with the high number of Cu entities present on the catalyst surface explain the measured higher activity of 4Cu−Al_2O_3. This candidate was therefore selected for further stability test and characterization studies.

Table 1. Cu/Al Atomic Ratio, BET Surface Area, Pore Volume, and Crystalline Size of the Catalysts

catalyst	Cu/Al atomic ratio[a]	S_{BET} (m^2 g^{-1})	V_p (cm^3 g^{-1})	crystalline size (nm)
2Cu−Al_2O_3	1.2	119.1	0.39	10[b]
4Cu−Al_2O_3	2.2	45.3	0.16	6[b]
6Cu−Al_2O_3	3.7	33.8	0.14	7[b]
Cu/Al_2O_3	0.1	117.3	0.23	3[b]
Cu/ZnO/Al_2O_3	1.3	84	0.24	5[b]
$CuAl_2O_4$	0.6	1.3	0.01	197[c]

[a]Determined with ICP-OES. [b]From the XRD pattern of CuO. [c]From the XRD pattern of $CuAl_2O_4$.

Figure 1a depicts the performance of the 4Cu−Al_2O_3 catalyst over 40 h on stream at T = 600 °C and WHSV= 300 000 mL g^{-1} h^{-1}. Using 4Cu−Al_2O_3 catalyst, 47% CO_2 conversion and 100% CO selectivity were achieved while no detectable deactivation was observed after 40 h of operation proving its remarkable activity and stability during the test (carbon balance and TPO shown in Figure S7).

In comparison, the reference catalyst, Cu/Al_2O_3, lost approximately 50% of its limited initial activity of 22% CO_2 conversion. Cu/ZnO/Al_2O_3 (HiFUEL W220, Alfa Aesar) was also tested for comparison due to its known WGS activity (temperature-programmed reduction (H_2-TPR) profile shown in Figure S8). This reference catalyst also lost 73% of its initial activity after 40 h. To compensate for the lower copper loading of the Cu/Al_2O_3 catalyst compared to 4Cu−Al_2O_3 (based on Cu wt % measured by ICP-OES), we have also tested the performance of these catalysts normalized to their amount of copper (Figure 1b). Despite the higher WHSV value, 4Cu−Al_2O_3 still outperformed the conventional supported Cu/Al_2O_3 catalyst in both activity and stability. Therefore, the observed higher activity of 4Cu−Al_2O_3 was not a consequence of the higher copper loading alone with the same active sites. We thus expected fundamental differences between the active sites of 4Cu−Al_2O_3 (due to surface Cu−Al spinel formation) and Cu/Al_2O_3. The CO_2 conversion rates for these catalysts are presented and compared to some of the literature reported catalysts in Table 2.

Better catalytic performance has been assigned to a strong metal−support interaction (SMSI) in many studies in the literature.[27−29] Therefore, we evaluated this possibility in our study through detailed characterization of the 4Cu−Al_2O_3 catalyst as well as the Cu/Al_2O_3 reference catalyst. To elucidate this interaction, H_2-TPR was conducted. On the basis of the results shown in Figure 2a, the H_2-TPR profile of 4Cu−Al_2O_3 showed three peaks while the last peak was not observed for Cu/Al_2O_3. The first two peaks were assigned to the well-dispersed copper oxide species and the bulk copper oxide crystals, respectively.[30,31] The last peak could be caused by the reduction of larger copper oxide entities in the bulk of 4Cu−Al_2O_3. In both cases, the first peak is independent of the crystal size. We observed that the first peak in the H_2-TPR profile significantly shifted to higher temperatures (200 °C) for 4Cu−Al_2O_3 compared to the same peak for Cu/Al_2O_3 (178 °C) supporting the strong influence of aluminum on copper in the 4Cu−Al_2O_3 catalyst, which can be described as the strong interaction of the well-dispersed copper oxide species on the catalyst surface with the support.[27,32,33]

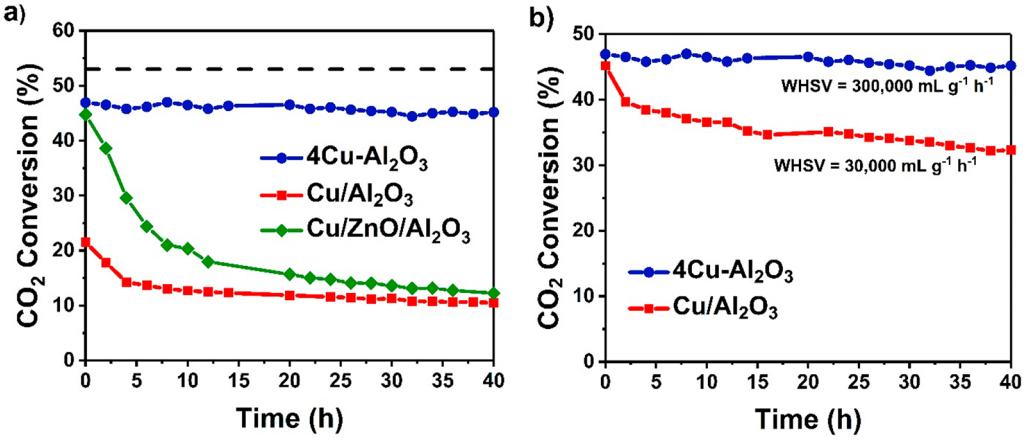

Figure 1. Comparison of CO_2 conversion using (a) 4Cu−Al_2O_3, Cu/Al_2O_3, and Cu/ZnO/Al_2O_3 at T = 600 °C and WHSV = 300 000 mL g^{-1} h^{-1}. Equilibrium at 600 °C: ∼53% (dashed line) (b) using 4Cu−Al_2O_3 and Cu/Al_2O_3 at T = 600 °C (WHSV adjusted to be proportional to the Cu loading: 300 000 mL g^{-1} h^{-1} for 4Cu−Al_2O_3 and 30 000 mL g^{-1} h^{-1} for Cu/Al_2O_3).

DOI: 10.1021/acscatal.9b01822
ACS Catal. 2019, 9, 6243−6251

Table 2. Comparison of the Catalysts Selectivity and CO_2 Conversion Rate, P = 1 atm

catalyst	temperature (K)	CO selectivity (%)	rate[a] ($\times 10^{-5}$ mol CO_2 g_{cat}^{-1} s^{-1})	Cu surface (m^2 g_{cat}^{-1})	ref
$4Cu-Al_2O_3$	873	100	17.9	–[b]	this work
Cu/Al_2O_3	873	100	4.9	4.3	this work
$Cu/ZnO/Al_2O_3$	873	100	7.6	28.4	this work
$CuAl_2O_4$	873	100	0.5	–[b]	this work
Co/β-Mo_2C	573	98.1	0.7		22
Cu/β-Mo_2C	873	99.2	14.2	4.2	11
BZYZ ($BaZr_{0.8}Y_{0.16}Zn_{0.04}O_3$)	873	97.0	0.2		9
$Pd-Fe/SiO_2$	723	97.2	0.3		23
$Cu-Fe/SiO_2$	873	NA	3.7	5.2	13
$Cu-K/SiO_2$	873	NA	7.3	5.1	24
Pt/CeO_2	563	NA	3.8		25
$PtCo/TiO_2$	573	99	0.6		26

[a]Calculated on the basis of eq 1 with data from this work and/or the references. [b]Not measurable with N_2O adsorption, since the surface consists of Cu^{2+} ions instead of metallic Cu.

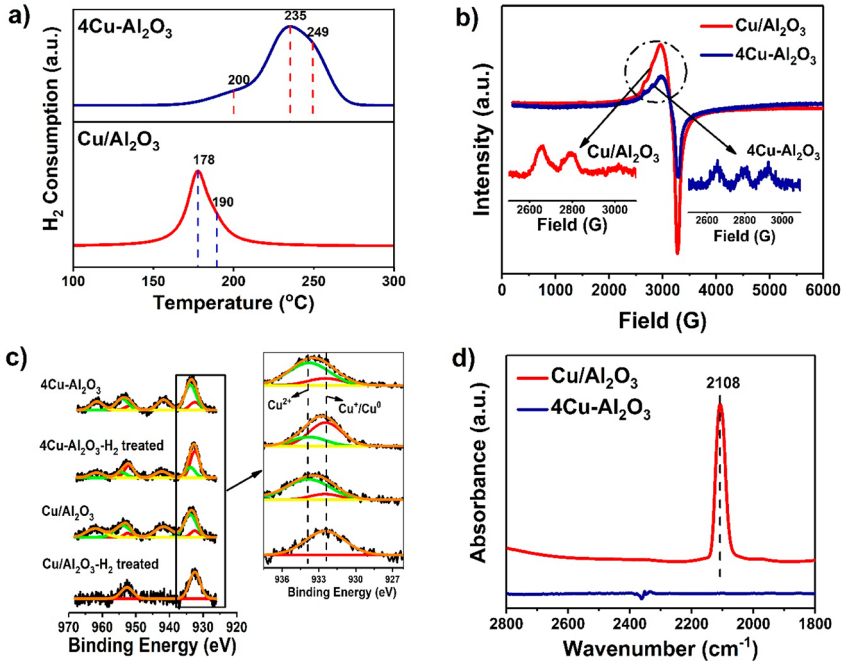

Figure 2. (a) H_2-TPR profiles for Cu/Al_2O_3 and $4Cu-Al_2O_3$. (b) EPR spectra for Cu/Al_2O_3 and $4Cu-Al_2O_3$ catalysts. The magnified parts show the baseline-subtracted hyperfine structures. (c) AP-XPS (Cu 2p) for Cu/Al_2O_3 and $4Cu-Al_2O_3$ before and after H_2 treatment (signal intensity multiplied by 3.5 and 13 for $4Cu-Al_2O_3$ and $4Cu-Al_2O_3-H_2$ treated, respectively). (d) CO–DRIFT spectra at room temperature for Cu/Al_2O_3 and $4Cu-Al_2O_3$.

We used electron paramagnetic resonance (EPR) to study the metal–support interaction and the catalyst structure in more detail. The spectral parameters ($g_\perp$ = 2.05, $g_\parallel$ = 2.34, $A_\parallel$ = 147 G) are known to be caused by the distorted octahedral coordination of Cu^{2+} ions.[34] The EPR spectrum of Cu/Al_2O_3 showed a higher signal intensity due to a higher concentration of Cu^{2+} ions obtained by the smaller CuO crystals and better Cu dispersion (Figure 2b). However, the hyperfine structure of $4Cu-Al_2O_3$ was better resolved. The resolution of the hyperfine structure is an indicator of the presence of the *isolated* Cu^{2+} ions where distinct peaks appear due to the lack of spin–spin interaction.[31,35] Isolated Cu^{2+} ions are known to strongly interact with the catalyst support.[31,36] This means that although there were fewer Cu^{2+} ions present in the $4Cu-Al_2O_3$ catalyst compared to Cu/Al_2O_3, they mainly consisted of isolated ions, which created a strong bond with the catalyst support and generated distinct peaks in the EPR hyperfine structure. The strong interaction of the isolated Cu^{2+} ions with Al_2O_3 can potentially lead to the formation of a surface Cu–Al spinel.[37]

To have a better understanding of the catalyst surface, ambient pressure X-ray photoelectron spectroscopy (AP-XPS) was applied (Figure 2c). Deconvolution of the acquired spectra for the Cu 2p 3/2 and Cu 2p 1/2 regions for both catalysts showed the presence of mainly a Cu^{2+} peak before hydrogen treatment (933.7 eV). After hydrogen treatment, the Cu^{2+} peak in the Cu/Al_2O_3 catalyst spectra completely disappeared showing full conversion of Cu^{2+} to Cu^0/Cu^+ (932.5 eV). However, the Cu^{2+} peak in the $4Cu-Al_2O_3$ catalyst spectra showed only a reduction in its intensity. The shakeup satellite peaks are final state effects associated with the presence of Cu^{2+}. Thus, their intensity is proportional to the presence/amount of Cu^{2+}. In agreement with the deconvolution of the main photoemission peaks, the shakeup satellite peak was

DOI: 10.1021/acscatal.9b01822
ACS Catal. 2019, 9, 6243–6251

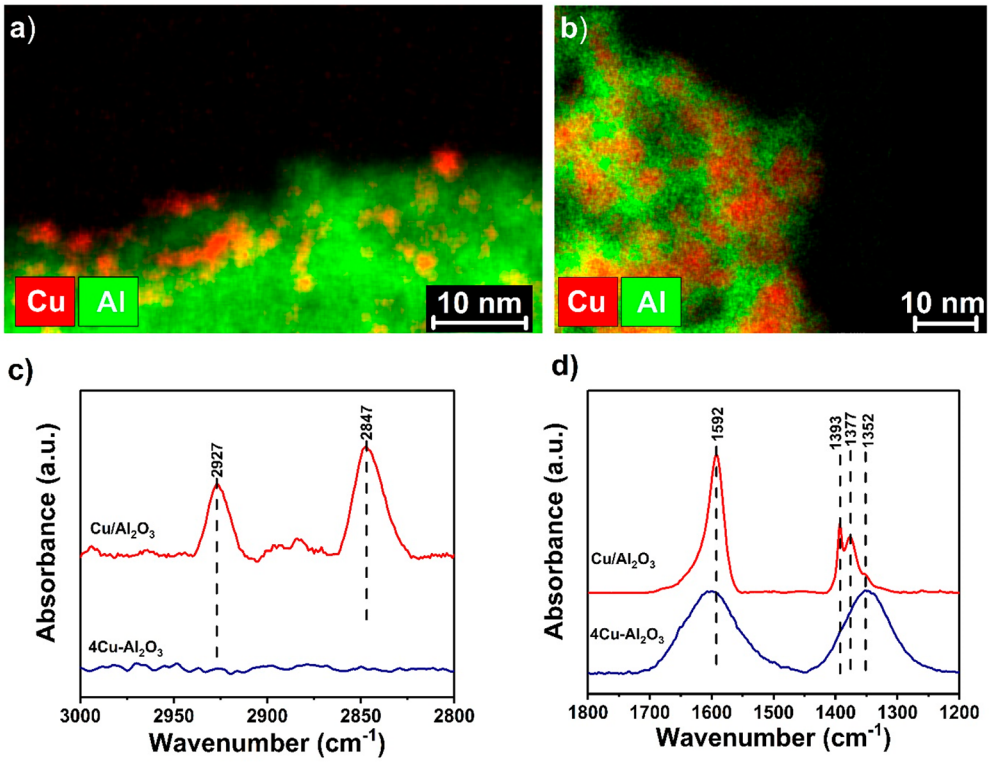

Figure 3. STEM-EDXS image of (a) the Cu/Al_2O_3 catalyst and (b) the $4Cu-Al_2O_3$ catalyst. (c, d) In situ DRIFTS spectra for Cu/Al_2O_3 and $4Cu-Al_2O_3$ catalysts.

partly preserved. Cu^{2+} was present on the $4Cu-Al_2O_3$ catalyst surface after hydrogen treatment at 300 °C, despite the fact that no reduction peak was detected at temperatures above 300 °C (and up to 800 °C) on the basis of the H_2-TPR experiment (Figure S9). This means that a phase change occurred on the catalyst surface (formation of Cu−Al spinel); otherwise, full reduction of the catalyst would have been expected.

The signal intensity was also considerably reduced after hydrogen treatment of $4Cu-Al_2O_3$ catalyst while the same phenomenon did not occur for Cu/Al_2O_3 (Figure S10). This could be an indication of Cu cation diffusion into the Al_2O_3 support during in situ formation of a Cu−Al spinel oxide on the surface of $4Cu-Al_2O_3$.[38] The majority of Cu^{2+} ions in a bulk Cu−Al spinel has a tetrahedral coordination, with higher binding energies compared to Cu^{2+} in the CuO structure. In comparison, Cu^{2+} ions in the surface-formed Cu−Al spinel mostly have a distorted octahedral coordination and possess binding energies similar to Cu^{2+} in the CuO structure.[39,40] Nonetheless, the presence of a Cu^0/Cu^+ peak on the $4Cu-Al_2O_3$ catalyst after hydrogen treatment was also noted on the basis of AP-XPS. Therefore, the oxidation state of the available copper for the reaction was investigated by diffuse reflectance infrared Fourier transform spectroscopy using CO as the probe molecule (CO−DRIFTS). After hydrogen pretreatment of both catalysts at 300 °C for 1 h, CO gas was dosed to the samples at room temperature and purged with Ar. A distinct peak of adsorbed CO on Cu/Al_2O_3 at 2108 cm^{-1} was observed (Figure 2d) which is the characteristic peak of adsorbed CO on Cu^0.[41] However, no CO adsorption whatsoever was detected on the surface of $4Cu-Al_2O_3$. This observation confirmed that the available surface of the catalyst consisted of a lean surface spinel, exclusively, since CO does not adsorb on Cu^{2+} in the Cu−Al spinel structure, unlike Cu^0 and Cu^+.[42]

To confirm the presence of Cu−Al spinel on the catalyst surface, the performance of this catalyst was compared to a reference Cu−Al spinel ($CuAl_2O_4$). Since the BET surface area of the $CuAl_2O_4$ catalyst was significantly lower compared to $4Cu-Al_2O_3$ (1.3 $m^2\ g^{-1}$ as opposed to 45.3 $m^2\ g^{-1}$), the amount of $CuAl_2O_4$ used for the reaction was chosen in a way to compensate for the lower surface area (procedure is described in the Methods section). CO_2 conversion using the $CuAl_2O_4$ catalyst was very close to the conversion achieved by using the $4Cu-Al_2O_3$ catalyst (Figure S11) which confirmed the in situ formation of the Cu−Al spinel on $4Cu-Al_2O_3$ surface. Elemental mapping of $4Cu-Al_2O_3$ further indicated a more homogeneous mixture of copper and aluminum in $4Cu-Al_2O_3$ compared to Cu/Al_2O_3 (Figure 3a,b). From this we concluded that the reason for the formation of the Cu−Al spinel phase on the $4Cu-Al_2O_3$ catalyst surface has to be found in the intimate contact between the two phases as well as the strong interaction of the isolated Cu^{2+} ions with alumina.

To investigate the active sites participating in the reaction, in situ adsorption of CO_2 and H_2 was studied using DRIFTS. C−H vibrating modes were monitored between 2800 and 3000 cm^{-1} (Figure 3c), and O−C−O stretching vibrational modes were monitored between 1300 and 1700 cm^{-1} (Figure 3d).[43] Peaks of O−C−O stretching vibrational modes were observed associated with CO_2 adsorption on both surfaces. However, it was difficult to assign the peaks observed in the wavenumber range 1300−1700 cm^{-1} to a specific molecular structure due to the very close wavenumber values of formate and carbonate in this range.[43−45] Nonetheless, distinctions between these components can be found in the C−H vibrating mode range (2800−3000 cm^{-1}).[46] The peaks observed in the C−H vibrating mode range for adsorbed CO_2 and H_2 on the Cu/Al_2O_3 surface clearly confirmed the formation of formate

DOI: 10.1021/acscatal.9b01822
ACS Catal. 2019, 9, 6243−6251

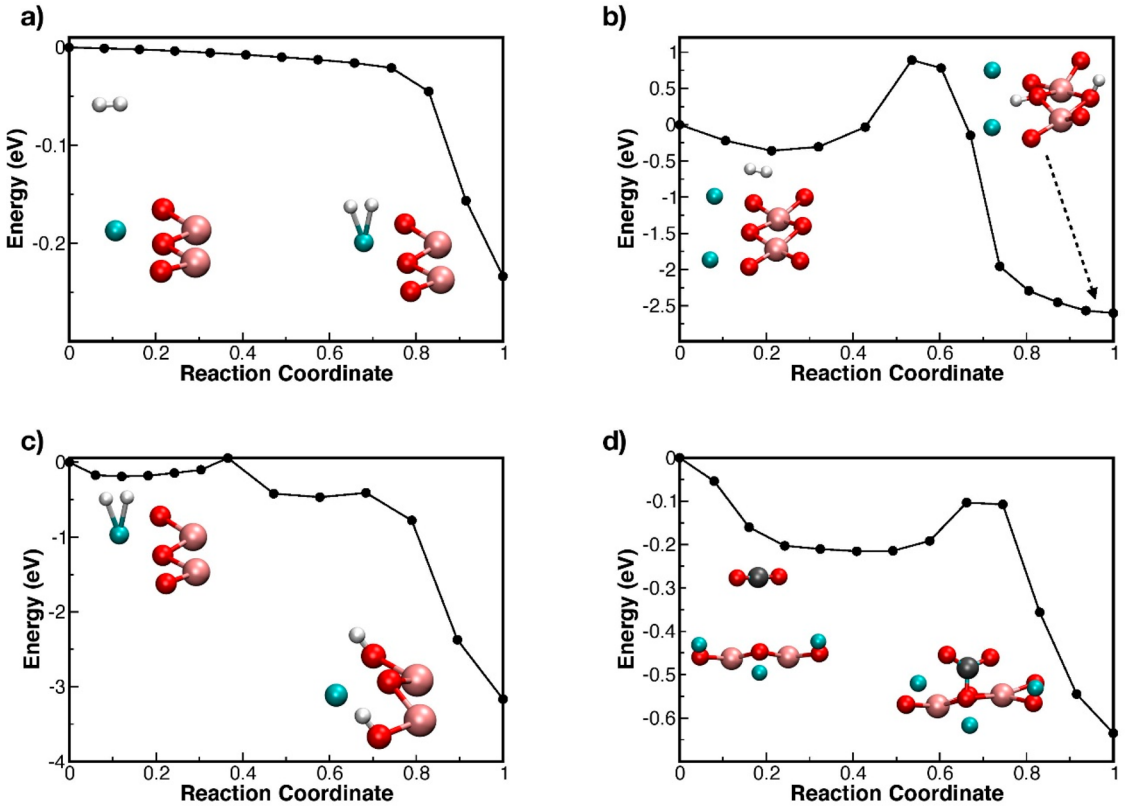

Figure 4. Minimum energy path (MEP) for (a) dissociation of the H_2 molecule over the Cu_{2f} atom, (b) dissociation of the H_2 molecule on the O_{3f} atom, (c) a dissociated H_2 molecule moving to two nearby O_{3f} atoms, and (d) adsorption of the CO_2 molecule on the O_{3f} atom of the $CuAl_2O_4$ surface.

species on the surface of this catalyst, while no C−H bond was observed after CO_2 and H_2 adsorption on the 4Cu−Al_2O_3 catalyst. Therefore, formation of carbonate species was supposed on the 4Cu−Al_2O_3 catalyst surface before addition of hydrogen and desorption from the surface.

To identify the active species for adsorption of CO_2 and H_2 on the 4Cu−Al_2O_3 catalyst surface, a density functional theory (DFT/PBE) study was performed. All calculations were performed on a Cu−Al spinel $CuAl_2O_4$ (100) surface with a (2 × 2 × 1) super cell. This surface was selected because it is the most stable low-index $CuAl_2O_4$ surface that can be cleaved from this structure (Figure S12).[47] We determined which possible surface adsorbates for H_2 and CO_2 were energetically favorable. Adsorption energies of the H_2 molecule and H atoms binding to doubly coordinated surface Cu ions (Cu_{2f}) as well as 3-fold and 4-fold coordinated surface oxygen atoms were calculated (Table S2). On the basis of the calculated adsorption energies, the dissociated adsorbed H_2 molecule on 3-fold coordinated surface oxygen (O_{3f}) atoms with a binding energy of −212 kJ mol^{-1} was found to be energetically most favorable. However, CI-NEB calculations showed that H_2 dissociation can occur spontaneously on Cu_{2f} (Figure 4a) while the dissociative adsorption of H_2 on O_{3f} was prevented by an energy barrier of 0.89 eV (Figure 4b). It was also found through these calculations that H migration from Cu_{2f} to two adjacent O_{3f} can occur almost spontaneously (Figure 4c).

Thus, although initial H_2 dissociation occurred on Cu_{2f}, the active species for further reaction was found to sit on O_{3f}. This thermodynamically driven migration to the oxygen sites explains why Cu^{2+} ions were not reduced upon H_2 exposure of the 4Cu−Al_2O_3 catalyst. Similarly, for the adsorption of CO_2, O_{3f} sites were energetically strongly preferred compared to O_{4f} and Cu_{2f} (Table S2 and Figure 4d) which is in agreement with the experimental observation of carbonate formation on the 4Cu−Al_2O_3 catalyst surface. Therefore, Cu_{2f} and O_{3f} were considered the catalyst's active sites participating in the RWGS reaction.

CONCLUSIONS

In many studies verifying the effect of copper impregnation on the metal oxide supports, it is reported that a high loading of copper (>5%) leads to weak copper−support interaction due to a poor copper dispersion.[32,48] Consequently, highly loaded copper catalysts are less stable and exhibit low catalytic activity. In contrast, we found that a coprecipitated 4Cu−Al_2O_3 catalyst is an excellent candidate for the RWGS reaction in terms of both stability and activity despite its high copper content per gram of catalyst. The characterization results of the coprecipitated 4Cu−Al_2O_3 catalyst revealed the presence of isolated Cu^{2+} ions and their strong interaction with alumina under a hydrogen stream, favoring the in situ Cu−Al spinel surface formation. Both Cu−Al spinel and the supported Cu nanoparticles (Cu/Al_2O_3 and $Cu/ZnO/Al_2O_3$) were active in the RWGS reaction. However, much higher activity and stability were observed in the case of Cu−Al spinel formation. DFT calculations suggested that while H_2 dissociation occurred on Cu^{2+} ions of the Cu−Al spinel surface, the most stable surface adsorbates for both H_2 and CO_2 was formed on O_{3f} sites. These sites, therefore, acted as the active sites for the catalytic hydrogenation of CO_2 to form CO. The combination of high activity and stability makes this catalyst an attractive

DOI: 10.1021/acscatal.9b01822
ACS Catal. 2019, 9, 6243−6251

candidate for use in chemical processes to utilize CO_2 in a future carbon recycling economy.

METHODS

Catalyst Preparation. The commercial $Cu/ZnO/Al_2O_3$ catalyst (HiFUEL W220, Alfa Aesar) and $CuAl_2O_4$ spinel (ABCR) were purchased and used as received. To prepare the coprecipitated nCu−Al_2O_3 catalysts with various Cu/Al atomic ratios, available protocols in the literature were followed.[49,50] The desired contents of copper and aluminum precursors, i.e., $Cu(NO_3)_2{\cdot}3H_2O$ (ABCR) and $Al(NO_3)_3{\cdot}9H_2O$ (Sigma-Aldrich), were dissolved in milli-Q water. Solutions (1.0 M) of NaOH and Na_2CO_3 were prepared and mixed together to form the precipitating agents. Metal precursor solution and the precipitating agents were added together dropwise while the basicity of the solution was kept constant at pH ∼ 9. The resulting suspension was stirred overnight at 75 °C. The precipitated mixture was filtered and washed until the pH of the filtrate reached ∼7. No sodium was detected through XPS analysis on the surface of these catalysts which showed that the catalysts were washed properly during this stage. The sample was then dried at 110 °C for 12 h and calcined at 600 °C for 6 h under static air (5 °C min^{-1}). The Cu/Al_2O_3 catalyst was prepared by wet impregnation method using copper precursor ($Cu(NO_3)_2{\cdot}3H_2O$) (ABCR) and γ-Al_2O_3 (Merck). The wet impregnation method is described elsewhere.[51]

Catalytic Tests. For each test, the desired amount of catalyst was placed between two quartz wool plugs in a fixed-bed quartz reactor. Each catalyst was first treated with hydrogen under 20 mL min^{-1} H_2 flow at 300 °C for 1 h. After hydrogen treatment, the gas flow was switched to pure Ar, and the reactor temperature was then set to the desired operating temperature. The reactor was working at atmospheric pressure for all catalytic tests. During the reaction, a 50 mL min^{-1} flow of CO_2 and H_2 (CO_2:H_2 = 1:2) was used, and the product stream was monitored using an on-line MATRIX-MG01 FTIR spectrometer (Bruker) equipped with OPUS-GA software and a 10 cm gas cell heated at 120 °C. To confirm the presence of Cu−Al spinel phase on the surface of the 4Cu−Al_2O_3 catalyst, the performance of this catalyst was compared to $CuAl_2O_4$ with equal surface area. Therefore, to compensate for the lower surface area of $CuAl_2O_4$ (1.3 m^2 g^{-1} as opposed to 45.3 m^2 g^{-1}), 0.348 g of $CuAl_2O_4$ was used in this test (as opposed to 0.01 g for 4Cu−Al_2O_3) with the same conditions as reported for the catalytic test. The commercial $Cu/ZnO/Al_2O_3$ catalyst was reduced under the same conditions as the other catalysts (under 20 mL min^{-1} H_2 flow for 1 h) but at 400 °C based on the H_2-TPR results (Figure S7). The CO_2 conversion rates were calculated on the basis of the following equation:

$$r = \frac{F \times X}{W} \tag{1}$$

with F being the CO_2 flow rate (mol s^{-1}), X the CO_2 conversion, and W the catalyst weight (g).

The carbon balance was calculated as follows:

$$C_{balance} = \frac{(CO)_{out} + (CO_2)_{out}}{(CO_2)_{in}} \tag{2}$$

with $(CO)_{out}$ and $(CO_2)_{out}$ being the molar flows of CO and CO_2 leaving the reactor (detected by FTIR), and $(CO_2)_{in}$ is the molar flow of the CO_2 in the bypass before switching to the reactor.

Catalyst Characterization. The Brunauer−Emmett−Teller (BET) surface, Barrett−Joyner−Halenda (BJH) mesoporous, and DFT microporous volumes were calculated from N_2-physisorption measurements on a Micromeritics 3Flex apparatus at liquid nitrogen temperature between 10^{-5} and 0.99 relative N_2 pressure. Samples (ca. 100 mg) were dried at 120 °C (temperature reached with a ramp of 2 °C min^{-1}) under vacuum (<10^{-3} mbar) for 4 h, and a leak test was performed prior to analysis.

Temperature-programmed reduction (TPR) was performed on a Micromeritics Autochem 2920 II instrument. Typically, the sample (ca. 100 mg) was loaded into a U-shaped cell and dried for 30 min under He flow (50 mL min^{-1}) at 150 °C (5 °C min^{-1}). After cooling down to 50 °C, the flow was switched to a 10:90 (volumetric ratio) H_2:Ar mixture, and temperature was ramped to 800 °C (10 °C min^{-1}). During this process, H_2 consumption was monitored using a calibrated thermal conductivity detector.

Elemental analyses by inductively coupled plasma optical emission spectroscopy (ICP-OES) were performed at the EPFL Central Environmental Laboratory on an ICPE-9000 Multitype Shimadzu instrument. From these measurements, the copper contents of the nCu−Al_2O_3 (n = 2, 4, 6) catalysts were determined as 35, 41, and 55 wt %, respectively. The Cu/Al_2O_3 catalyst contained 4 wt %, commercial $Cu/ZnO/Al_2O_3$ 42 wt %, and the $CuAl_2O_4$ spinel catalysts 33 wt % copper, respectively.

Determination of the copper surface area for $Cu/ZnO/Al_2O_3$ and Cu/Al_2O_3 was done on a Micromeritics Autochem II 2920 instrument using N_2O as a reactive probe selective to metallic surface Cu atoms according to the method described by Vannice et al.[41] A 0.2 g portion of each sample was reduced in situ (same method as TPR) and contacted with 0.5 mL N_2O pulses using a sampling loop carried by a flow of He at 90 °C while N_2 evolution and N_2O consumption were quantified by monitoring masses 28 and 44, respectively, using an MKS Cirrus 2 mass spectrometer.

High-angle annular dark-field scanning transmission electron microscopy (HAADF-STEM) was conducted on an FEI Talos instrument with 200 kV acceleration voltage in the mode resulting in atomic number contrast (Z contrast). Samples were dispersed in ethanol and placed on the carbon-coated gold grid. Energy-dispersive X-ray spectroscopy (EDXS) analysis was performed using Bruker Esprit software.

DRIFT spectra were recorded using a high-temperature Harrick DRIFT cell on a PerkinElmer Frontier spectrometer equipped with a mercury cadmium telluride detector. Spectra were typically collected with 32 scans at a resolution of 4 cm^{-1}. For CO adsorption, the sample was pretreated at 120 °C (1 °C min^{-1}) under helium (100 mL min^{-1}) for 1 h. After cooling down to 15 °C, the sample was exposed to CO flow (100 mL min^{-1}) for 5 min, and excess CO was eliminated by flowing helium (100 mL min^{-1}) for 30 min. The in situ reaction was carried out by flowing a CO_2/H_2 mixture (100 mL min^{-1}) at 250 °C. The excess gas mixture was then purged by flowing helium for 30 min.

Small-angle XRD measurements were performed in a PANalytical Empyrean system (Theta−Theta, 240 mm) equipped with parallel beam mirror optics and Cu Kα radiation.

Ambient pressure X-ray photoelectron spectroscopy (AP-XPS) measurements were carried out at the ISS (in situ spectroscopy) end station operated at the X07DB beamline

DOI: 10.1021/acscatal.9b01822
ACS Catal. 2019, 9, 6243−6251

(Swiss light source, Paul Scherrer Institute, Villigen PSI). Linearly polarized light was used, and the excitation energy was set to 1250 eV. The spectra were acquired with a Scienta R4000 Hipp-2 spectrometer, using 50 eV pass energy, a dwell time of 0.1 s, and a step size of 100 meV. The spectra were normalized to the number of sweeps, aligned using the C 1s signal as a reference, (284.5 eV) and peak deconvolution was done using Voigt-shaped peaks after subtraction of a Shirley background. During the deconvolution of all the Cu 2p spectra, the position, the full width at half-maximum, and the line shape (% of Lorentian and Gaussian) were constrained.

The powder was dispersed in isopropanol and then drop-cast on a silver foil. The sample was mounted on an IR laser heated (λ = 915 nm, $Power_{max}$ = 25 W) manipulator, where the focused laser hits the back side of the sample holder, and the temperature is measured with a Pt1000 sensor. The samples were introduced in vacuum; then, the measurement cell was isolated, and all the spectra were acquired stabilizing the background pressure at 1.0 mbar. An inert gas (He) was used to limit the charging during the characterization of the as-introduced sample, and the temperature was kept constant at 50 °C. Then, the gas was switched to hydrogen (1.0 mbar), and the samples were annealed in situ at 300 °C for 1 h. After the pretreatment, the samples were cooled down to 50 °C in hydrogen, and the photoemission spectra were acquired again. The Cu 2p spectra of both catalysts were deconvoluted according to the literature.[52,53] Two doublets were used to fit the main peak (Cu $2p_{3/2}$) and its spin−orbit satellite (Cu $2p_{1/2}$), and a third doublet was used to fit the shakeup satellites located in the 940−945 and 960−965 eV binding energy regions.

Computational Methods. All density functional theory (DFT) calculations were performed using the Quantum Espresso package.[54] The generalized gradient approximation (GGA) with parametrization due to Perdew−Burke−Ernzerhof (PBE) was used for the exchange correlation functional.[55] Ultrasoft pseudopotentials were used to describe the interaction between the (semi)valence electrons and the nuclei and core electrons for all of the atoms. Kohn−Sham orbitals and the total electronic density were expanded in a plane wave basis with energy cutoffs of 130 and 630 Ry, respectively.

We sampled a (1 × 1 × 1) cell with 10 Å vacuum to separate periodic images with a 4 × 4 × 1 Monkhorst−Pack *k*-point grid while (2 × 2 × 1) super cells with the same vacuum separation were modeled with a 2 × 2 × 2 *k*-point mesh.[56] These values were chosen by checking the convergence of the total energy (~10^{-3} Ry $atom^{-1}$) and atomic forces (~10^{-4} Ry au^{-1}).

A surface model (100) including eight layers of $CuAl_2O_4$ (containing 224 atoms) was built. The entire model was optimized in a box of 16.52 × 16.52 × 18.26 Å.

The adsorption energies per molecule were calculated from the following relation:

$$E_{ads} = E_{(surf+mol)} - (E_{surf} + E_{mol})$$

where $E_{(surf+mol)}$ is the total energy of the adsorbate−substrate system, E_{mol} is the energy of the isolated molecule, and E_{surf} is the energy of the surface. We used the improved CI-NEB method to calculate the activation energy barriers.[57]

■ ASSOCIATED CONTENT

Supporting Information

The Supporting Information is available free of charge on the ACS Publications website at DOI: 10.1021/acscatal.9b01822.

Catalytic tests, N_2 physisorption data, XRD patterns, STEM-EDXS images, catalyst surface composition, carbon balance and TPO, H_2-TPR profiles, AP-XPS raw spectra, comparison with reference $CuAl_2O_4$, modeled $CuAl_2O_4$ surface, and calculated adsorption energies (PDF)

■ AUTHOR INFORMATION

Corresponding Author

*E-mail: oliver.kroecher@psi.ch.

ORCID

Ali M. Bahmanpour: 0000-0003-2092-9215
Luca Artiglia: 0000-0003-4683-6447
Ursula Röthlisberger: 0000-0002-1704-8591
Jeremy S. Luterbacher: 0000-0002-0967-0583
Oliver Kröcher: 0000-0002-7268-7257

Notes

The authors declare no competing financial interest.

■ ACKNOWLEDGMENTS

This research project is part of the Swiss Competence Center for Energy Research SCCER BIOSWEET of the Swiss Innovation Agency Innosuisse. F.H. and J.S.L. acknowledge funding from the Swiss National Science Foundation through Grant PYAPP2_154281. The authors would like to acknowledge D. Alexander for STEM-EDXS analysis, A. Sienkiewicz for EPR analysis, P. Schouwink for XRD analysis, and S. Coudret for ICP-OES analysis. M.K. and U.R. acknowledge HPC resources of CSCS (Swiss National Supercomputer Centre).

■ REFERENCES

(1) MacDowell, N.; Florin, N.; Buchard, A.; Hallett, J.; Galindo, A.; Jackson, G.; Adjiman, C. S.; Williams, C. K.; Shah, N.; Fennell, P. An Overview of CO_2 Capture Technologies. *Energy Environ. Sci.* **2010**, *3*, 1645−1669.

(2) Wang, W.; Wang, S.; Ma, X.; Gong, J. Recent Advances in Catalytic Hydrogenation of Carbon Dioxide. *Chem. Soc. Rev.* **2011**, *40*, 3703−3727.

(3) Wang, X.; Shi, H.; Szanyi, J. Controlling Selectivities in CO_2 reduction through Mechanistic Understanding. *Nat. Commun.* **2017**, *8*, 513.

(4) Wang, W. H.; Himeda, Y.; Muckerman, J. T.; Manbeck, G. F.; Fujita, E. CO_2 Hydrogenation to Formate and Methanol as an Alternative to Photo- and Electrochemical CO_2 Reduction. *Chem. Rev.* **2015**, *115*, 12936−12973.

(5) Chinchen, G. C.; Denny, P. J.; Jennings, J. R.; Spencer, M. S.; Waugh, K. C. Synthesis of Methanol. Part 1. Catalysts and Kinetics. *Appl. Catal.* **1988**, *36*, 1−65.

(6) Herman, R. G.; Klier, K.; Simmons, G. W.; Finn, B. P.; Bulko, J. B.; Kobylinski, T. P. Catalytic Synthesis of Methanol from CO H_2. I. Phase Composition, Electronic Properties, and Activities of the Cu/ZnO/M_2O_3 Catalysts. *J. Catal.* **1979**, *56*, 407−429.

(7) Kwak, J. H.; Kovarik, L.; Szanyi, J. Heterogeneous Catalysis on Atomically Dispersed Supported Metals: CO_2 Reduction on Multifunctional Pd Catalysts. *ACS Catal.* **2013**, *3*, 2094−2100.

(8) Fisher, I. A.; Bell, A. T. A Comparative Study of CO and CO_2 hydrogenation over Rh/SiO_2. *J. Catal.* **1996**, *162*, 54−65.

DOI: 10.1021/acscatal.9b01822
ACS Catal. 2019, 9, 6243−6251

(9) Kim, D. H.; Park, J. L.; Park, E. J.; Kim, Y. D.; Uhm, S. Dopant Effect of Barium Zirconate-Based Perovskite-Type Catalysts for the Intermediate-Temperature Reverse Water Gas Shift Reaction. *ACS Catal.* **2014**, *4*, 3117−3122.
(10) Yang, X.; Su, X.; Chen, X.; Duan, H.; Liang, B.; Liu, Q.; Liu, X.; Ren, Y.; Huang, Y.; Zhang, T. Promotion Effects of Potassium on the Activity and Selectivity of Pt/Zeolite Catalysts for Reverse Water Gas Shift Reaction. *Appl. Catal., B* **2017**, *216*, 95−105.
(11) Zhang, X.; Zhu, X.; Lin, L.; Yao, S.; Zhang, M.; Liu, X.; Wang, X.; Li, Y.-W.; Shi, C.; Ma, D. Highly Dispersed Copper over β-Mo2C as an Efficient and Stable Catalyst for the Reverse Water Gas Shift (RWGS) Reaction. *ACS Catal.* **2017**, *7*, 912−918.
(12) Álvarez Galván, C.; Schumann, J.; Behrens, M.; Fierro, J. L. G.; Schlögl, R.; Frei, E. Reverse Water-Gas Shift Reaction at the Cu/ZnO Interface: Influence of the Cu/Zn Ratio on Structure-Activity Correlations. *Appl. Catal., B* **2016**, *195*, 104−111.
(13) Chen, C. S.; Cheng, W. H.; Lin, S. S. Study of Iron-Promoted Cu/SiO_2 Catalyst on High Temperature Reverse Water Gas Shift Reaction. *Appl. Catal., A* **2004**, *257*, 97−106.
(14) Chen, C. S.; Lin, J. H.; You, J. H.; Chen, C. R. Properties of $Cu(thd)_2$ as a Precursor to Prepare Cu/SiO_2 Catalyst Using the Atomic Layer Epitaxy Technique. *J. Am. Chem. Soc.* **2006**, *128*, 15950−15951.
(15) Alejandre, A.; Medina, F.; Salagre, P.; Fabregat, A.; Sueiras, J. E. Characterization and Activity of Copper and Nickel Catalysts for the Oxidation of Phenol Aqueous Solutions. *Appl. Catal., B* **1998**, *18*, 307−315.
(16) Li, G.; Gu, C.; Zhu, W.; Wang, X.; Yuan, X.; Cui, Z.; Wang, H.; Gao, Z. Hydrogen Production from Methanol Decomposition Using Cu-Al Spinel Catalysts. *J. Cleaner Prod.* **2018**, *183*, 415−423.
(17) Tanaka, Y.; Utaka, T.; Kikuchi, R.; Takeguchi, T.; Sasaki, K.; Eguchi, K. Water Gas Shift Reaction for the Reformed Fuels over Cu/MnO Catalysts Prepared via Spinel-Type Oxide. *J. Catal.* **2003**, *215*, 271−278.
(18) Tanaka, Y.; Takeguchi, T.; Kikuchi, R.; Eguchi, K. Influence of Preparation Method and Additive for Cu-Mn Spinel Oxide Catalyst on Water Gas Shift Reaction of Reformed Fuels. *Appl. Catal., A* **2005**, *279*, 59−66.
(19) Xi, H.; Hou, X.; Liu, Y.; Qing, S.; Gao, Z. Cu-Al Spinel Oxide as an Efficient Catalyst for Methanol Steam Reforming. *Angew. Chem., Int. Ed.* **2014**, *53*, 11886−11889.
(20) Bolt, H. Transition Metal Aluminate Formation in Alumina-Supported Model Catalysts: High-Energy Ion Beam Analysis of Interfacial Processes, Chapters 5 and 6, Ph.D. Thesis, University of Utrecht, Netherlands, 1994.
(21) Mane, R. B.; Rode, C. V. Simultaneous Glycerol Dehydration and in Situ Hydrogenolysis over Cu-Al Oxide under an Inert Atmosphere. *Green Chem.* **2012**, *14*, 2780−2789.
(22) Porosoff, M. D.; Yang, X.; Boscoboinik, J. A.; Chen, J. G. Molybdenum Carbide as Alternative Catalysts to Precious Metals for Highly Selective Reduction of CO_2 to CO. *Angew. Chem., Int. Ed.* **2014**, *53*, 6705−6709.
(23) Park, J. N.; McFarland, E. W. A Highly Dispersed $Pd-Mg/SiO_2$ Catalyst Active for Methanation of CO_2. *J. Catal.* **2009**, *266*, 92−97.
(24) Chen, C. S.; Cheng, W. H.; Lin, S. S. Study of Reverse Water Gas Shift Reaction by TPD, TPR and CO_2 Hydrogenation over Potassium-Promoted Cu/SiO_2 Catalyst. *Appl. Catal., A* **2003**, *238*, 55−67.
(25) Goguet, A.; Meunier, F.; Breen, J. P.; Burch, R.; Petch, M. I.; Faur Ghenciu, A. Study of the Origin of the Deactivation of a Pt/CeO_2 Catalyst during Reverse Water Gas Shift (RWGS) Reaction. *J. Catal.* **2004**, *226*, 382−392.
(26) Kattel, S.; Yu, W.; Yang, X.; Yan, B.; Huang, Y.; Wan, W.; Liu, P.; Chen, J. G. CO_2 Hydrogenation over Oxide-Supported PtCo Catalysts: The Role of the Oxide Support in Determining the Product Selectivity. *Angew. Chem., Int. Ed.* **2016**, *55*, 7968−7973.
(27) Kim, M. S.; Chung, S. H.; Yoo, C. J.; Lee, M. S.; Cho, I. H.; Lee, D. W.; Lee, K. Y. Catalytic Reduction of Nitrate in Water over $Pd-Cu/TiO_2$ Catalyst: Effect of the Strong Metal-Support Interaction (SMSI) on the Catalytic Activity. *Appl. Catal., B* **2013**, *142−143*, 354−361.
(28) Kumar, A.; Ramani, V. Strong Metal-Support Interactions Enhance the Activity and Durability of Platinum Supported on Tantalum-Modified Titanium Dioxide Electrocatalysts. *ACS Catal.* **2014**, *4*, 1516−1525.
(29) Chen, P.; Khetan, A.; Yang, F.; Migunov, V.; Weide, P.; Stürmer, S. P.; Guo, P.; Kähler, K.; Xia, W.; Mayer, J.; Pitsch, H.; Simon, U.; Muhler, M. Experimental and Theoretical Understanding of Nitrogen-Doping-Induced Strong Metal-Support Interactions in Pd/TiO_2 Catalysts for Nitrobenzene Hydrogenation. *ACS Catal.* **2017**, *7*, 1197−1206.
(30) Bridier, B.; López, N.; Pérez-Ramírez, J. Partial Hydrogenation of Propyne over Copper-Based Catalysts and Comparison with Nickel-Based Analogues. *J. Catal.* **2010**, *269*, 80−92.
(31) Dow, W. P.; Wang, Y. P.; Huang, T. J. Yttria-Stabilized Zirconia Supported Copper Oxide Catalyst: I. Effect of Oxygen Vacancy of Support on Copper Oxide Reduction. *J. Catal.* **1996**, *160*, 155−170.
(32) Sagar, G. V.; Rao, P. V. R.; Srikanth, C. S.; Chary, K. V. R. Dispersion and Reactivity of Copper Catalysts Supported on Al_2O_3-ZrO_2. *J. Phys. Chem. B* **2006**, *110*, 13881−13888.
(33) Huang, T. J.; Yu, T. C.; Chang, S. H. Effect of Calcination Atmosphere on CuO/γ-Al_2O_3 Catalyst for Carbon Monoxide Oxidation. *Appl. Catal.* **1989**, *52*, 157−163.
(34) Tikhov, S. F.; Sadykov, V. A.; Kryukova, G. N.; Paukshtis, E. A.; Popovskii, V. V.; Starostina, T. G.; Kharlamov, G. V.; Anufrienko, V. F.; Poluboyarov, V. F.; Razdobarov, V. A.; Bulgakov, N. N.; Kalinkin, A. V. Microstructural and Spectroscopic Investigations of the Supported Copperalumina Oxide System: Nature of Aging in Oxidizing Reaction Media. *J. Catal.* **1992**, *134*, 506−524.
(35) Wang, X.; Shi, Y.; Li, S.; Li, W. Promotional Synergistic Effect of Cu and Nb Doping on a Novel Cu/Ti-Nb Ternary Oxide Catalyst for the Selective Catalytic Reduction of NO_x with NH_3. *Appl. Catal., B* **2018**, *220*, 234−250.
(36) Dumas, J. M.; Geron, C.; Kribii, A.; Barbier, J. Preparation of Supported Copper Catalysts. II. Reduction of Copper/Alumina Catalysts. *Appl. Catal.* **1989**, *47*, L9−L15.
(37) Yan, J. Y.; Lei, G. D.; Sachtler, W. M. H.; Kung, H. H. Deactivation of Cu/ZSM-5 Catalysts for Lean NO_x Reduction: Characterization of Changes of Cu State and Zeolite Support. *J. Catal.* **1996**, *161*, 43−54.
(38) Fernández-García, M.; Gómez Rebollo, E.; Guerrero Ruiz, A.; Conesa, J. C.; Soria, J. Influence of Ceria on the Dispersion and Reduction/Oxidation Behaviour of Alumina-Supported Copper Catalysts. *J. Catal.* **1997**, *172*, 146−159.
(39) Strohmeier, B. R.; Levden, D. E.; Field, R. S.; Hercules, D. M. Surface Spectroscopic Characterization of Cu/Al_2O_3 Catalysts. *J. Catal.* **1985**, *94*, 514−530.
(40) Friedman, R. M.; Freeman, J. J.; Lytle, F. W. Characterization of Cu/Al_2O_3 catalysts. *J. Catal.* **1978**, *55*, 10−28.
(41) Dandekar, A.; Vannice, M. A. Determination of the Dispersion and Surface Oxidation States of Supported Cu Catalysts. *J. Catal.* **1998**, *178*, 621−639.
(42) Davydov, A. Study of Cation States by DRES and FTIR Spectroscopies of the Probe Molecules. In *Molecular Spectroscopy of Oxide Catalyst Surfaces*; John Wiley & Sons, Ltd, 2003; pp 187−275.
(43) Kalamaras, C. M.; Olympiou, G. G.; Efstathiou, A. M. The Water-Gas Shift Reaction on Pt/γ-Al_2O_3 Catalyst: Operando SSITKA-DRIFTS-Mass Spectroscopy Studies. *Catal. Today* **2008**, *138*, 228−234.
(44) Demoulin, O.; Navez, M.; Ruiz, P. Investigation of the Behaviour of a Pd/γ-Al_2O_3 catalyst during Methane Combustion Reaction Using in Situ DRIFT Spectroscopy. *Appl. Catal., A* **2005**, *295*, 59−70.
(45) Ferreira-Aparicio, P.; Márquez-Alvarez, C.; Rodríguez-Ramos, I.; Schuurman, Y.; Guerrero-Ruiz, A.; Mirodatos, C. A Transient Kinetic Study of the Carbon Dioxide Reforming of Methane over Supported Ru Catalysts. *J. Catal.* **1999**, *184*, 202−212.

DOI: 10.1021/acscatal.9b01822
ACS Catal. 2019, 9, 6243−6251

(46) Jacobs, G.; Williams, L.; Graham, U.; Thomas, G. A.; Sparks, D. E.; Davis, B. H. Low Temperature Water-Gas Shift: In Situ DRIFTS-Reaction Study of Ceria Surface Area on the Evolution of Formates on Pt/CeO_2 Fuel Processing Catalysts for Fuel Cell Applications. *Appl. Catal., A* **2003**, *252*, 107−118.
(47) Zhang, Y.; Zhao, H.; Guo, L.; Zheng, C. Decomposition Mechanisms of Cu-Based Oxygen Carriers for Chemical Looping with Oxygen Uncoupling Based on Density Functional Theory Calculations. *Combust. Flame* **2015**, *162*, 1265−1274.
(48) Kwak, J. H.; Tonkyn, R.; Tran, D.; Mei, D.; Cho, S. J.; Kovarik, L.; Lee, J. H.; Peden, C. H. F.; Szanyi, J. Size-Dependent Catalytic Performance of CuO on γ-Al_2O_3: NO Reduction versus NH_3 Oxidation. *ACS Catal.* **2012**, *2*, 1432−1440.
(49) Velu, S.; Sabde, D. P.; Shah, N.; Sivasanker, S. New Hydrotalcite-like Anionic Clays Containing Zr^{4+} in the Layers: Synthesis and Physicochemical Properties. *Chem. Mater.* **1998**, *10*, 3451−3458.
(50) Zhang, J.; Chen, J. Selective Transfer Hydrogenation of Biomass-Based Furfural and 5-Hydroxymethylfurfural over Hydrotalcite-Derived Copper Catalysts Using Methanol as a Hydrogen Donor. *ACS Sustainable Chem. Eng.* **2017**, *5*, 5982−5993.
(51) Bahmanpour, A. M.; Hoadley, A.; Tanksale, A. Formaldehyde Production via Hydrogenation of Carbon Monoxide in the Aqueous Phase. *Green Chem.* **2015**, *17*, 3500−3507.
(52) Frost, D. C.; Ishitani, A.; McDowell, C. A. X-Ray Photoelectron Spectroscopy of Copper Compounds. *Mol. Phys.* **1972**, *24*, 861−877.
(53) Biesinger, M. C. Advanced Analysis of Copper X-Ray Photoelectron Spectra. *Surf. Interface Anal.* **2017**, *49*, 1325−1334.
(54) Giannozzi, P.; Baroni, S.; Bonini, N.; Calandra, M.; Car, R.; Cavazzoni, C.; Ceresoli, D.; Chiarotti, G. L.; Cococcioni, M.; Dabo, I.; Corso, A. D.; de Gironcoli, S.; Fabris, S.; Fratesi, G.; Gebauer, R.; Gerstmann, U.; Gougoussis, C.; Kokalj, A.; Lazzeri, M.; MartinSamos, L.; Marzari, N.; Mauri, F.; Mazzarello, R.; Paolini, S.; Pasquarello, A.; Paulatto, L.; Sbraccia, C.; Scandolo, S.; Sclauzero, G.; Seitsonen, A. P.; Smogunov, A.; Umari, P.; Wentzcovitch, R. M. QUANTUM ESPRESSO: A Modular and Open-Source Software Project for Quantum Simulations of Materials. *J. Phys.: Condens. Matter* **2009**, *21*, 395502.
(55) Perdew, J. P.; Burke, K.; Wang, Y. Generalized Gradient Approximation for the Exchange-Correlation Hole of a Many-Electron System. *Phys. Rev. B: Condens. Matter Mater. Phys.* **1996**, *54*, 16533−16539.
(56) Monkhorst, H. J.; Pack, J. D. Special Points for Brillouin-Zone Integrations. *Phys. Rev. B* **1976**, *13*, 5188−5192.
(57) Henkelman, G.; Uberuaga, B. P.; Jónsson, H. Climbing Image Nudged Elastic Band Method for Finding Saddle Points and Minimum Energy Paths. *J. Chem. Phys.* **2000**, *113*, 9901−9904.

DOI: 10.1021/acscatal.9b01822
ACS Catal. 2019, 9, 6243−6251